International Journal of
Molecular Sciences

MDPI

Article

Yeast as a Platform to Dissect Poly(ADP-Ribose) Polymerase Function from *Magnaporthe oryzae* and Evaluate PARP Inhibitors

Rachel E. Kalicharan, Nalleli Payne and Jessie Fernandez *

Department of Microbiology and Cell Science, Institute of Food and Agricultural Sciences, University of Florida, Gainesville, FL 32611, USA; rkalicharan@ufl.edu (R.E.K.); ngarciarodriguez@ufl.edu (N.P.)
* Correspondence: jessie.fernandez@ufl.edu

Abstract

Poly(ADP-ribose) polymerases (PARPs) regulate genome maintenance through NAD^+-dependent ADP-ribosylation, yet PARP function in fungi remains poorly defined. Here, we reconstituted the activity of the *Magnaporthe oryzae* PARP1 homolog (MoPARP1) in *Saccharomyces cerevisiae*, a genetically tractable organism that lacks endogenous PARP enzymes. Upon galactose induction, expression of MoPARP1 reduced yeast growth, whereas a catalytically inactive mutant showed no defect, indicating that the growth phenotype depends on PARP catalytic activity. Consistent with this requirement, PARylation was detected in MoPARP1-expressing yeast cells but not in the catalytic mutant. In a multidrug transporter-deficient background, the PARP inhibitor 3-aminobenzamide and the clinically used PARP inhibitor olaparib rescued the growth of MoPARP1-expressing strains, establishing a framework for inhibitor testing in vivo. Finally, MoPARP1-GFP localized to the nucleus independent of catalytic activity, supporting correct targeting in this heterologous system. Together, these findings establish yeast as a platform to dissect fungal PARP biology and evaluate chemical inhibition.

Keywords: PARylation; PARP1; yeast; *Magnaporthe oryzae*; inhibitor

1. Introduction

Poly(ADP-ribose) polymerases (PARPs) are a large and diverse family of ADP-ribosyltransferases (ARTs) found across eukaryotes. Using nicotinamide adenine dinucleotide (NAD^+) as a substrate, PARPs transfer ADP-ribose units onto target proteins, adding either a single ADP-ribose unit through mono-ADP-ribosylation (MARylation) or multiple ADP-ribose units to form poly(ADP-ribose) (PAR) chains (PARylation) [1–4]. In humans, at least 17 PARP family members have been identified. PARP1, the most abundant and best-studied family member, catalyzes the majority of DNA damage-induced PAR synthesis and regulates DNA repair, chromatin dynamics, transcription, and cell death [5]. Human PARP1 is a modular enzyme containing regulatory motifs and accessory domains, including zinc finger DNA-binding domains, the tryptophan-glycine-arginine (WGR) domain, and a BRCA1 C-terminal (BRCT) domain, together with a conserved catalytic domain characterized by the histidine-tyrosine-glutamate (HYE) motif [3,6]. PAR signals are reversed primarily by poly(ADP-ribose) glycohydrolase (PARG) and can be pharmacologically blocked using PARP inhibitors [6,7]. Disruption of PARP-mediated ADP-ribosylation is associated with neurodegeneration, metabolic dysfunction, inflammatory diseases, and cancer [4,8]. Notably, the finding that PARP1/2 inhibition can selectively kill BRCA-deficient tumor cells led to the development of multiple FDA-approved PARP

Check for updates

Academic Editor: Maurizio Ciani

Received: 30 December 2025
Revised: 11 February 2026
Accepted: 14 February 2026
Published: 16 February 2026

Copyright: © 2026 by the authors. Licensee MDPI, Basel, Switzerland. This article is an open access article distributed under the terms and conditions of the Creative Commons Attribution (CC BY) license.

inhibitors [9–11]. These advances underscore the importance of defining PARP enzymology and the mechanisms by which ADP-ribosylation supports cellular homeostasis. Despite extensive characterization of human PARPs, far less is known about PARP function across other eukaryotic lineages. Plants encode multiple PARP homologs implicated in DNA damage responses and genome maintenance, and they also contribute to broader stress-response signaling [12–14].

Interest in PARP biology has recently expanded to filamentous fungi, where biological roles have been difficult to dissect, in part because few systems enable robust in vivo biochemical interrogation. Of particular interest is *Magnaporthe oryzae,* the rice blast fungus. Rice blast is one of the most globally devastating agricultural diseases, destroying up to 30% of harvested rice annually [15,16]. This disease is especially difficult to combat due to the hemibiotrophic lifestyle of *M. oryzae*, which allows the pathogen to proliferate within the host in a symptomless manner during its biotrophic phase for the first 48 hours of infection [17]. The fungal pathogen will then switch to the necrotrophic phase, characterized by cell death, which manifests as necrotic lesions that ultimately render the crop unusable [18]. To initiate the disease cycle, *M. oryzae*'s three-celled conidium will land on the leaf surface, often transported by natural elements like wind, rain, or irrigation. Upon sensing surface cues of the leaf, the conidium will germinate and eventually form an appressorium [19]. Appressorium formation is a critical step in the disease cycle, as it facilitates mechanical penetration into the host, followed by hyphal dissemination intercellularly [20]. It is now becoming increasingly evident that PARP activity and PARylation are not only present in *M. oryzae*, but also integral to the fungus' pathogenicity. MoPARP1 mediates PARylation of 14-3-3 proteins, regulating appressorium development, mitogen-activated protein kinase (MAPK) signaling, and virulence, ultimately implicating ADP-ribosylation in infection-structure differentiation and host invasion [21]. Similar impacts have been documented in other phytopathogenic fungi, including *Fusarium oxysporum* f. sp. *niveum*. In this species, FonPARP1 is an active nuclear PARP whose activity is enhanced by kinase-dependent phosphorylation, and it mediates substrate-specific PARylation of the protein disulfide isomerase FonPdi1, thereby regulating protein folding, endoplasmic reticulum homeostasis, and pathogenicity [22,23]. These studies position fungal PARPs as virulence-linked regulators, supporting a reductionist approach to evaluating PARP catalytic outputs and chemical sensitivity in a simplified cellular background.

Heterologous gene expression in yeast provides a powerful approach to define PARP function [24]. Prior studies have characterized human and plant PARPs in *Saccharomyces cerevisiae* [25–27]. Because yeast lacks endogenous PARP genes and does not synthesize PAR, it offers a genetically "clean" background in which all detected ADP-ribosylation is derived from the introduced enzyme. This genetic simplicity, combined with tractable manipulation and the absence of endogenous PARylation machinery, makes yeast a uniquely useful platform for reconstructing and interrogating PARP activities from diverse organisms.

In this study, we reconstitute and characterize the *M. oryzae* PARP1 homolog (MoPARP1) in the PARP-free background of *S. cerevisiae*. We demonstrate that induced expression of MoPARP1 in yeast results in a strong, catalytic activity-dependent growth defect, detectable PARylation activity, and nuclear localization. A catalytic-site mutant abolishes all enzymatic and phenotypic outputs, confirming dependence on the conserved glutamate residue required for ADP-ribosyltransferase activity. Finally, we show that MoPARP1 is inhibited in vivo by mammalian PARP inhibitors, 3-aminobenzamide and olaparib, establishing a foundation for using yeast as a screening platform for inhibitors targeting fungal PARPs. Together, our results provide the first biochemical reconstruction of fungal PARP activity in yeast and introduce a versatile system for functional analysis and discovery of antifungal inhibitors.

2. Results

2.1. Expression of MoPARP1 Reduces Yeast Growth in a Catalytic-Dependent Manner

To assess whether expression of *M. oryzae* PARP1 (MoPARP1) affects yeast growth, we analyzed *S. cerevisiae* BY4741 strains carrying an empty vector (EV), wild-type MoPARP1, or a catalytically inactive mutant (MoPARP1-E714A), targeting a conserved glutamate residue in the PARP active site that is essential for NAD^+ binding and ADP-ribose transfer, under repressing (glucose) and inducing (galactose) conditions [1,14,28,29]. Human PARP1 (HsPARP1) was included as a reference for PARP-dependent growth defects previously described in yeast [26,30].

Under repressing conditions, all strains displayed comparable growth across serial dilutions, indicating that basal expression did not measurably impact growth (Figure 1A). Upon galactose induction, expression of MoPARP1 resulted in a marked reduction in colony formation across the dilutions relative to EV controls. To verify that the observed growth phenotypes were associated with induced PARP expression, we analyzed protein levels by immunoblotting using an anti-MYC antibody. MoPARP1 and MoPARP1-E714A were readily detected at the expected molecular weight in galactose-induced cultures, whereas no signal was observed under repressing conditions or in EV controls (Figure 1B). In contrast, the expression of the catalytic mutant MoPARP1-E714A did not reduce growth, with colony formation comparable to EV on both glucose and galactose media (Figure 1A). These observations indicate that MoPARP1-dependent growth inhibition in yeast requires an intact catalytic residue.

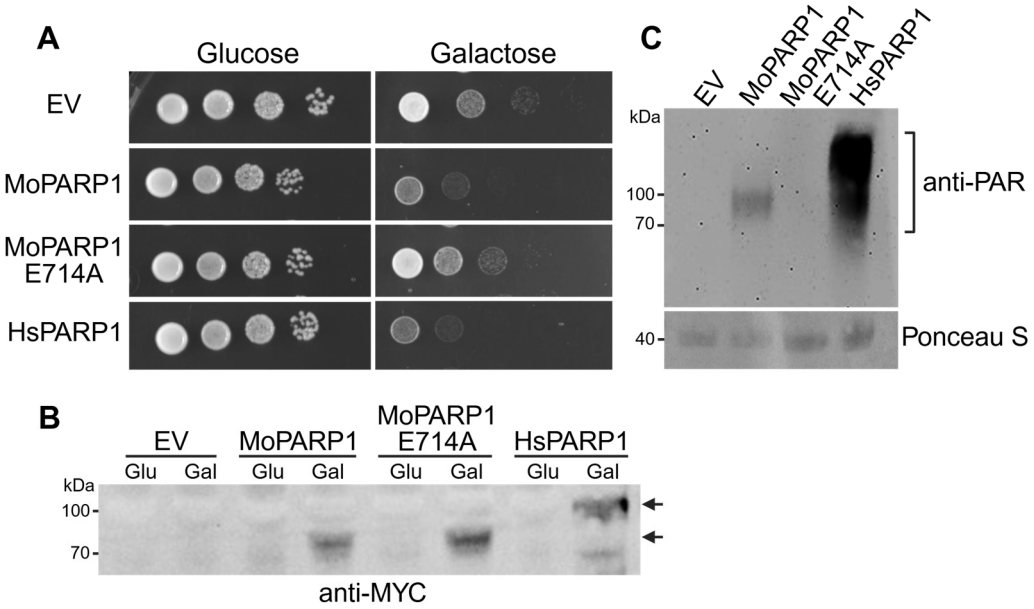

Figure 1. Galactose-inducible expression of PARP1 fusion proteins in yeast and verification of expression. (**A**) BY4741 yeast strains expressing the empty vector (EV) or indicated PARP1-MYC fusion constructs were grown overnight in repressing medium (2% glucose). Cultures were normalized to an OD_{600} of 0.5, serially diluted 10-fold, and spotted onto plates containing either repressing medium (2% glucose) or inducing medium (2% galactose). Plates were imaged after 2 days of incubation at 30 °C. (**B**) Induced cultures from (**A**) were harvested at equal cell equivalents, lysed, and analyzed by SDS-PAGE followed by immunoblotting with an anti-MYC antibody to confirm expression at the expected molecular weights as indicated by the black arrows (MoPARP1, 87 kDa; HsPARP1, 110 kDa). (**C**) PARylation analysis of yeast expressing PARP1 constructs. Galactose-induced cells were treated with 0.05% MMS for 3 h, followed by Af1521 macrodomain enrichment and immunoblotting with anti-PAR antibody. Equal loading was confirmed with Ponceau S of the Af1521 macrodomain fusion protein.

Consistent with prior reports, the induction of HsPARP1 expression resulted in strong growth inhibition on galactose plates (Figure 1A). Notably, MoPARP1 expression produced a qualitatively similar growth phenotype, supporting functional similarity between fungal and human PARP proteins in this heterologous system.

2.2. MoPARP1 Catalyzes PARylation in Yeast Cells

To determine whether MoPARP1 functions as an active PARP in vivo, we analyzed PAR formation in yeast protein extracts by immunoblotting using anti-PAR antibodies. While PARylation can be detected in mammalian cells and is enhanced by DNA-damaging agents such as methyl methanesulfonate (MMS), we were unable to detect PARylation in whole-cell lysates of yeast expressing MoPARP1 following galactose induction and treatment with 0.05% MMS. This indicates that overall PARylation levels in yeast are below the detection limit of standard immunoblotting approaches, as previously reported [31]. Therefore, we employed an enrichment strategy using Af1521 macrodomain affinity purification to selectively isolate ADP-ribosylated proteins prior to analysis [31]. Macrodomain-coupled agarose beads were used to pull down PARylated proteins from yeast lysates, including auto-PARylated MoPARP1, thereby increasing the sensitivity of PAR detection.

Using this enrichment approach, PARylated proteins were detected in yeast cells expressing wild-type MoPARP1 (Figure 1C). In contrast, no PARylation signal was observed in EV controls or in strains expressing the catalytically inactive MoPARP1-E714A mutant, demonstrating that PARylation depends on an intact catalytic glutamate residue. As expected, expression of human PARP1 resulted in a strong PARylation signal, serving as a positive control for PARylation activity in yeast. Together, these results demonstrate that MoPARP1 catalyzes PARylation in yeast cells and that its enzymatic activity depends on a conserved catalytic residue. These biochemical data are consistent with and support the catalytic-dependent growth phenotype observed in the spotting assay (Figure 1A).

2.3. MoPARP1 Expression Alters Growth Dynamics in Liquid Culture

To further characterize growth behavior, we monitored growth dynamics in liquid culture. Under glucose conditions, all strains exhibited similar growth kinetics (Figure 2A,B), consistent with the results of the spotting assay and confirming that the phenotype depends on induced expression. In galactose conditions, strains expressing MoPARP1 or HsPARP1 exhibited a reproducible, pronounced growth delay and achieved lower maximal optical densities compared to EV controls (Figure 2C,D). In contrast, MoPARP1-E714A displayed growth kinetics comparable to EV, consistent with its established effects in yeast. Quantification of growth curves by area under the curve (AUC) analysis supported these observations, with reduced AUC values for MoPARP1- and HsPARP1-expressing strains relative to controls, while MoPARP1-E714A showed no significant difference (Figure 2C,D). Notably, MoPARP1-E714A displayed a modestly extended lag phase prior to exponential growth, although overall growth, as measured by AUC, was comparable to the EV control. Together, these data demonstrate that MoPARP1 impairs yeast growth in a catalytic activity-dependent manner, producing a growth phenotype comparable to that observed upon expression of HsPARP1.

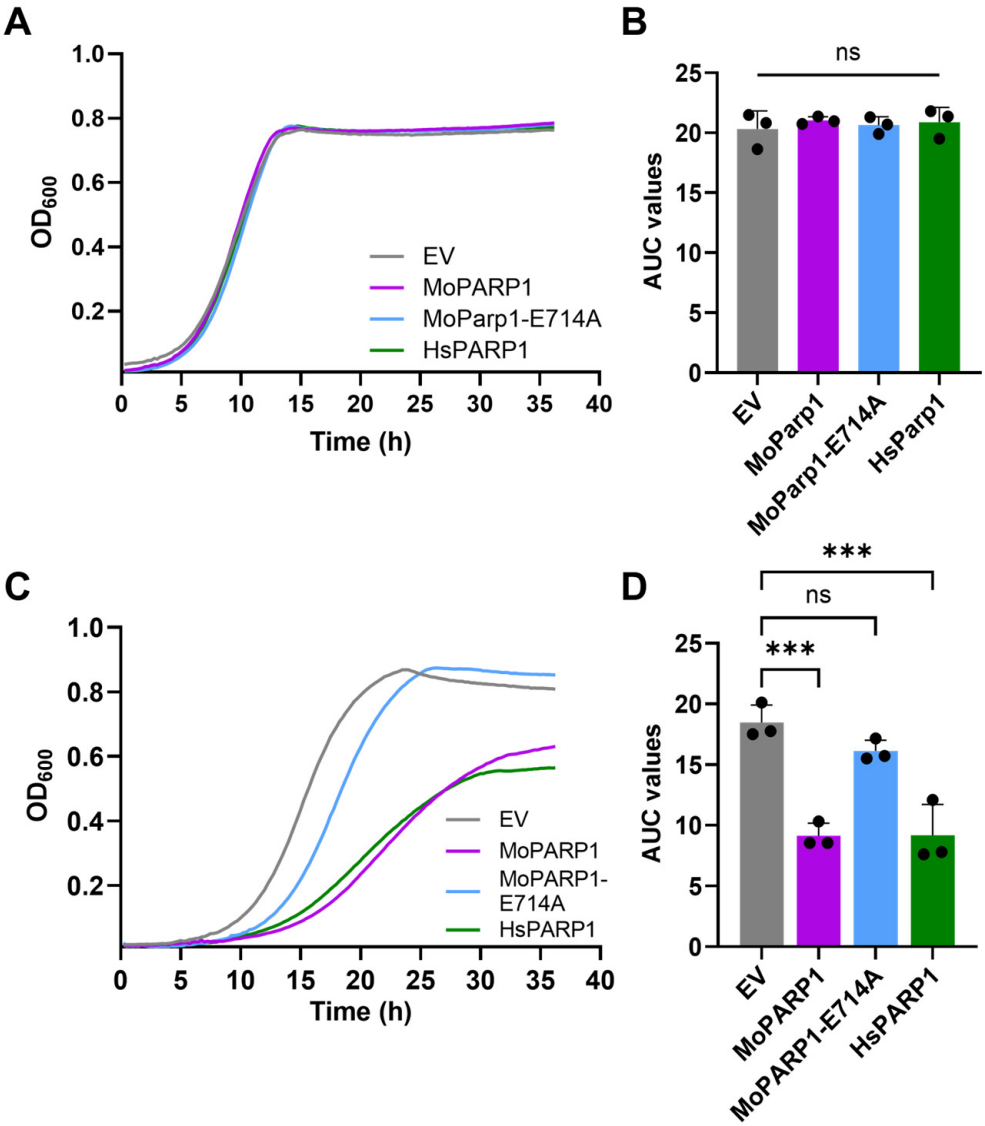

Figure 2. MoPARP1 inhibits yeast growth in a catalytic-dependent manner. (**A**) OD_{600} growth curves of *S. cerevisiae* BY4741 expressing empty vector (EV), MoPARP1, catalytic mutant MoPARP1-E714A, or human PARP1 (HsPARP1) under repressing conditions (glucose). (**B**) Area under the curve (AUC) analysis of (**A**) shows no significant differences. (**C**) Under inducing conditions (galactose), expression of MoPARP1 and HsPARP1 reduced yeast growth compared with EV, whereas MoPARP1-E714A showed no significant effect. (**D**) AUC quantification of (**C**). MoPARP1 and HsPARP1 significantly reduced growth relative to EV, while MoPARP1-E714A did not. Each dot represents an independent biological replicate ($n = 3$), calculated as the mean of three technical replicates. Bars indicate mean ± SD. Statistical significance was determined by one-way ANOVA with Dunnett's multiple comparisons test; ***, $p < 0.001$; ns, not significant.

2.4. PARP Inhibitor Treatment Restores MoPARP1-Dependent Growth Inhibition in Yeast

To validate whether the growth inhibition associated with MoPARP1 expression is driven by PARP enzymatic activity, we examined the effect of pharmacological PARP inhibition in yeast. These experiments were performed in a BY4741-*pdr5*Δ background, which lacks a major ATP-binding cassette multidrug efflux transporter and thereby enhances intracellular accumulation of small molecules.

As observed in the wild-type background, induction of MoPARP1 expression in BY4741-*pdr5*Δ cells resulted in strong growth inhibition on galactose-containing media (Figure 3A,B). The addition of the PARP inhibitor 3-aminobenzamide (3-AB, 5 mM), a clas-

sical NAD$^+$ analog that inhibits PARP catalytic activity, restored the growth of MoPARP1-expressing strains, as evidenced by improved colony formation and enhanced growth in liquid culture (Figure 3A,B). In contrast, the growth of the strain expressing the catalytically inactive MoPARP1-E714A mutant was unaffected by 3-AB treatment, consistent with the absence of PARP catalytic activity in this variant.

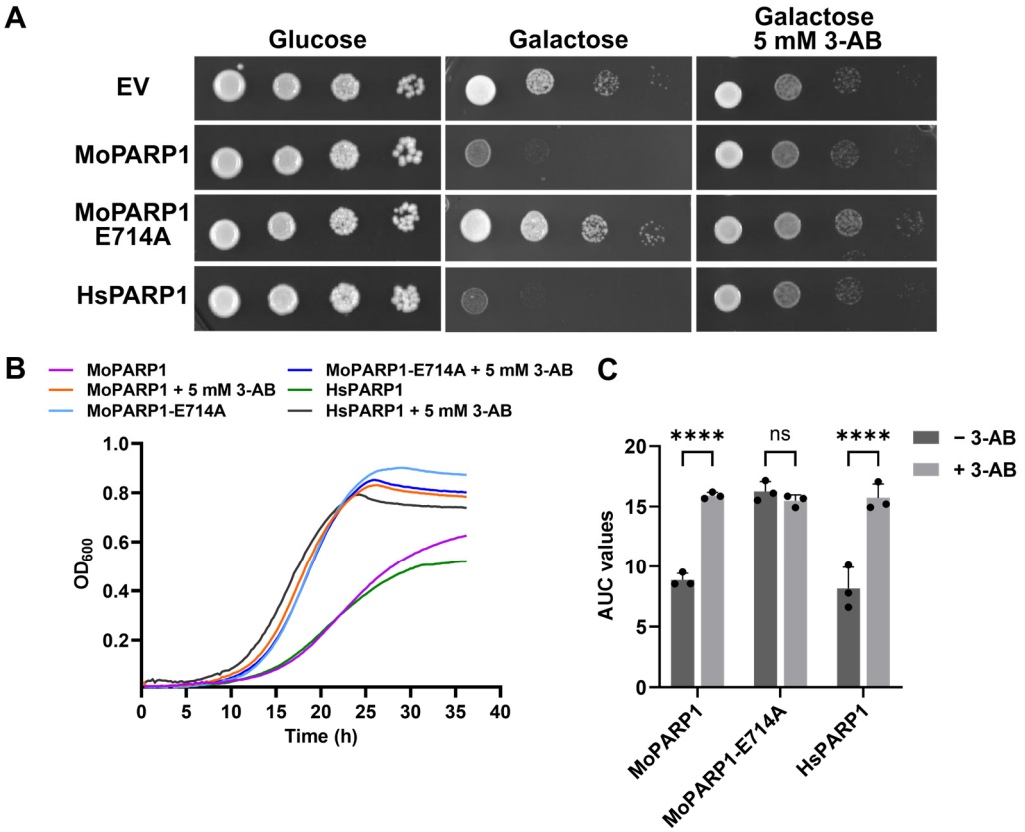

Figure 3. PARP inhibition rescues MoPARP1-mediated growth inhibition under inducing conditions. (**A**) Serial dilution spot assays of BY4741-*pdr5*Δ expressing empty vector (EV), MoPARP1, catalytic mutant MoPARP1-E714A, or HsPARP1. Cells were grown on glucose (repressing) or galactose (inducing) media in the presence or absence of 5 mM 3-aminobenzamide (3-AB). (**B**) Liquid growth curves (OD_{600}) under inducing conditions ± 5 mM 3-AB. (**C**) Area under the curve (AUC) quantification of (**B**). 3-AB significantly increased growth of MoPARP1-expressing cells but had no significant effect on MoPARP1-E714A. Each dot represents an independent biological replicate (n = 3), calculated as the mean of three technical replicates. Bars indicate mean ± SD. Statistical significance was determined by two-way ANOVA with Šídák's multiple comparisons test; ****, $p < 0.0001$; ns, not significant.

In line with its established behavior in yeast, the expression of HsPARP1 also caused strong growth inhibition, which was similarly alleviated by 3-AB treatment, serving as a positive control for PARP inhibitor responsiveness (Figure 3A,B). Quantitative analysis of growth curves using AUC measurements confirmed statistically significant restoration of growth for MoPARP1- and HsPARP1-expressing strains upon 3-AB treatment, whereas no significant change was observed for the catalytic mutant (Figure 3B,C).

To extend these findings using a mechanistically distinct inhibitor, we tested olaparib, a clinically used HsPARP1 inhibitor that targets the conserved NAD$^+$-binding pocket of the PARP catalytic domain. Under galactose-inducing conditions, treatment with 25 µM olaparib increased the growth of wild-type MoPARP1-expressing yeast in liquid culture relative to untreated controls (Figure 4A,B). This rescue was supported by AUC-based quantification, which showed a significant increase in AUC upon olaparib treatment ($p < 0.0001$).

A similar growth restoration was observed in yeast expressing HsPARP1, indicating that olaparib effectively suppresses PARP-dependent growth inhibition mediated by both fungal and human PARP1 in this heterologous system. In contrast, olaparib treatment had no significant effect on the growth of cells expressing the catalytically inactive MoPARP1-E714A mutant, consistent with the absence of PARP-dependent toxicity in this strain (Figure 4A,B). Together with the results obtained using 3-AB, these data indicate that MoPARP1-dependent growth inhibition in yeast is enzymatic in nature and can be mitigated by pharmacological PARP inhibition. Collectively, these results demonstrate that MoPARP1-dependent growth inhibition in yeast can be chemically modulated by PARP inhibitors. The concordant inhibitor responses further support functional conservation of key features of the PARP catalytic mechanism and establish yeast as a tractable platform for assessing pharmacological sensitivity of fungal PARP activity.

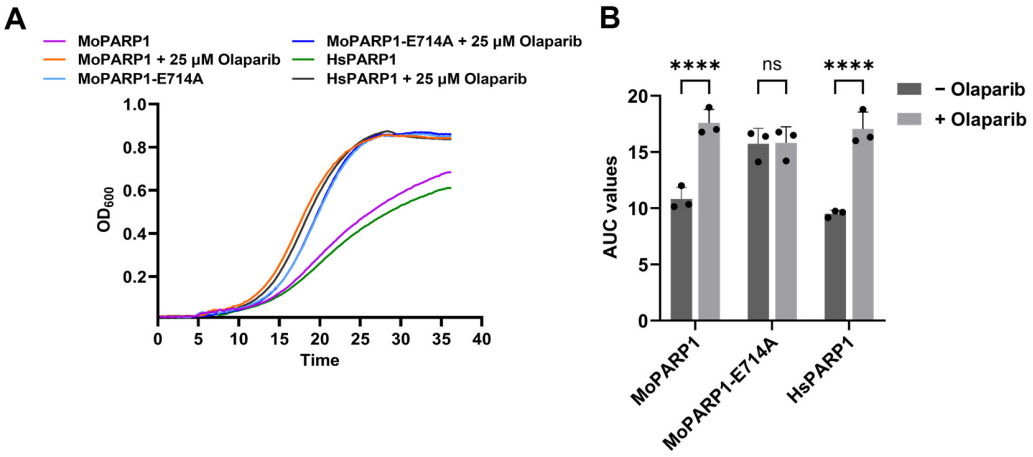

Figure 4. Effect of the PARP inhibitor olaparib on MoPARP1-dependent growth under inducing conditions. (**A**) Liquid growth curves (OD_{600}) of BY4741-*pdr5*Δ cells expressing MoPARP1, MoPARP1-E714A, or human PARP1 (HsPARP1) grown under galactose-inducing conditions in the absence or presence of olaparib (25 μM). (**B**) Area under the curve (AUC) quantification of the growth curves shown in (**A**). Each dot represents an independent biological replicate ($n = 3$), calculated as the mean of three technical replicates. Bars indicate mean ± SD. Statistical significance was determined by two-way ANOVA with Šídák's multiple-comparisons test; ****, $p < 0.0001$; ns, not significant.

2.5. MoPARP1 Localizes to the Nucleus in Yeast Independent of Its Catalytic Activity

To validate the yeast heterologous system and determine whether catalytic activity influences subcellular localization, we examined MoPARP1 localization in *S. cerevisiae*. Wild-type MoPARP1 and a catalytically inactive mutant, MoPARP1-E714A, were expressed as C-terminal GFP fusion proteins from a galactose-inducible vector in BY4741 cells. Fluorescence microscopy showed that both MoPARP1-GFP and MoPARP1-E714A-GFP localized exclusively to the nucleus, as indicated by the overlap with Hoechst staining and no detectable cytoplasmic signal (Figure 5). These results confirm correct nuclear targeting of MoPARP1 in yeast and indicate that differences in growth phenotypes between the wild-type and catalytic mutant proteins are not due to altered subcellular localization.

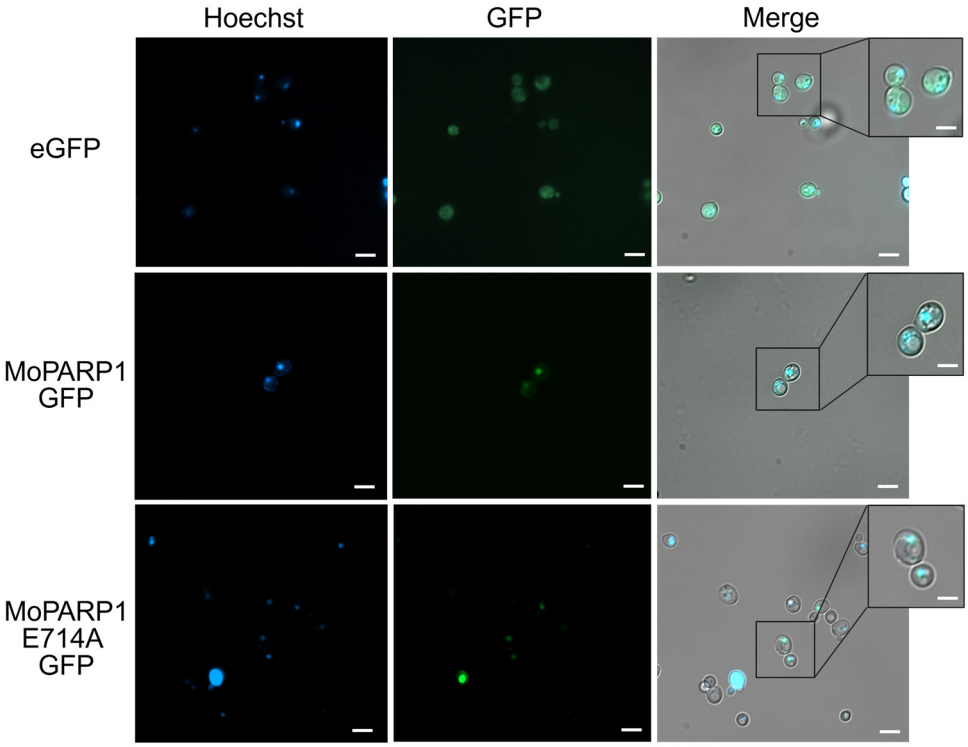

Figure 5. Subcellular localization of galactose-inducible MoPARP1-GFP fusion proteins in BY4741 yeast cells. BY4741 cells expressing galactose-inducible MoPARP1-GFP fusion constructs were grown under inducing conditions (galactose) and analyzed by fluorescence microscopy. eGFP fluorescence (green) was used to visualize the subcellular distribution of MoPARP1. Nuclei were stained with Hoechst 33342 (blue) as a nuclear marker. Merged images display the spatial relationship between MoPARP1-GFP and nuclear staining. Boxed regions indicate areas shown at higher magnification in the inset panels to highlight subcellular localization. Representative fluorescence and corresponding brightfield images are shown. Scale bars: 10 µm (main panels) and 5 µm (inset panels).

3. Discussion

Yeast heterologous expression systems provide a powerful way to dissect protein function in a simplified eukaryotic context, particularly for enzymatic activities that are absent from *S. cerevisiae* and therefore lack confounding endogenous regulation. Because yeast lacks canonical poly(ADP-ribose) polymerases, it provides an essentially background-free platform for isolating PARP-dependent effects and directly connecting catalytic activity to cellular phenotypes [24,25,32,33].

PARylation is a highly dynamic post-translational modification that can rapidly reshape protein interactions, chromatin organization, and stress-responsive signaling. Because PARP activity is tightly coupled to NAD^+ utilization and generates an amplifying biochemical output, even modest deregulation of PARylation can impose substantial fitness costs. In this context, yeast offers a controlled eukaryotic system in which PARP activity can be examined independently of organism-specific developmental programs or signaling networks. Here, we leverage this system to evaluate the cellular consequences of induced *M. oryzae* PARP1 expression, focusing on growth behavior, subcellular localization, and pharmacological sensitivity.

Using this approach, expression of wild-type MoPARP1 in yeast wielded a pronounced fitness cost, evident in both spot dilution assays and liquid growth curves, whereas growth under repressing conditions remained unaffected. These observations indicate that MoPARP1 is enzymatically active in vivo and that its activity alone is sufficient to disrupt cellular growth in a heterologous eukaryotic system, consistent with PARylation detected

in MoPARP1-expressing yeast and its absence in the catalytically inactive MoPARP1-E714A mutant. Comparable growth inhibition phenotypes have been reported upon expression of plant and mammalian PARPs in yeast, supporting the idea that deregulated PARP activity is intrinsically deleterious when uncoupled from native regulatory constraints [25,30,34]. However, it remains unknown which downstream processes are affected by MoPARP1 activity. Given the link between PARP activity and NAD^+ consumption, future work should investigate whether the growth defect results from NAD^+ depletion/metabolic stress, and whether it activates yeast stress-response pathways. This conclusion is further supported by analysis of the MoPARP1-E714A variant, which carries a substitution of a conserved catalytic glutamate within the PARP active site. This residue is required for NAD^+-dependent ADP-ribose transfer in PARP family enzymes, and its substitution is widely used to generate catalytically inactive PARP variants [1,14,23,28]. Consistent with loss of enzymatic activity, expression of MoPARP1-E714A did not impair yeast growth under inducing conditions, indicating that the observed fitness cost depends on an intact catalytic center rather than protein expression.

The modest lag-phase extension observed for MoPARP1-E714A likely reflects a transient protein expression burden, a well-documented phenomenon in yeast heterologous systems, rather than altered catalytic activity [35,36]. Importantly, this does not compromise the utility of the yeast platform, which remains a robust in vivo system for assessing MoPARP1 activity and for screening PARP inhibitors, as evidenced by reproducible inhibitor-mediated rescue of growth phenotypes.

The nuclear localization of MoPARP1 in yeast further supports its functional relevance in this system and is consistent with the established chromatin-associated roles of PARP proteins across eukaryotes. MoPARP1 accumulated predominantly in the nucleus under inducing conditions, indicating that nuclear targeting is preserved in the heterologous background. PARP localization has also been examined in *M. oryzae*, where PARP1-GFP fluorescence was readily detected in the nuclei of hyphal cells, while nuclear localization in three-celled conidia was not clearly observed under the conditions tested [21]. The conserved nuclear enrichment observed in hyphae and in yeast supports the view that nuclear targeting is an intrinsic property of MoPARP1 and reinforces the relevance of yeast as a system for assessing MoPARP1 localization and function. It remains unclear whether nuclear localization is required for MoPARP1-mediated toxicity and whether specific chromatin-associated interactions underline the observed growth defects.

Chemical inhibition experiments further support the enzymatic basis of the MoPARP1-dependent growth phenotype. Treatment with 3-AB and the human PARP inhibitor olaparib alleviated MoPARP1-dependent growth inhibition in a multidrug transporter-deficient (*pdr5*Δ) background, consistent with suppression of PARP catalytic activity. 3-AB is a classical competitive PARP inhibitor that binds the conserved nicotinamide-binding pocket within the NAD^+ site, thereby blocking ADP-ribosyl transfer. The ability to chemically modulate MoPARP1 activity in yeast further highlights the utility of this system for probing PARP enzymatic function. These inhibitor-rescue experiments raise questions about which features of the MoPARP1 catalytic domain govern inhibitor sensitivity and whether other clinically relevant PARP inhibitors (PARPis) show similar activity against fungal PARPs.

PARPis have become an important class of targeted therapeutics, particularly in ovarian cancer, and several agents, including olaparib, niraparib, and rucaparib, are approved by the U.S. Food and Drug Administration for maintenance therapy [9]. Olaparib was the first PARPi approved as first-line maintenance monotherapy based on the phase III trial. Mechanistically, olaparib binds to the conserved NAD^+-binding pocket of PARP enzymes, inhibiting catalytic PARylation and also stabilizing PARP-DNA complexes, thereby promot-

ing DNA damage repair in cells with PARP deficiency [7]. Because olaparib is well studied clinically and mechanistically, it provides a useful pharmacological probe for assessing PARP-dependent phenotypes. In the context of this study, the responsiveness of MoPARP1 to olaparib further supports conservation of key catalytic features and validates the use of yeast as a platform for probing fungal PARP activity.

More broadly, yeast has been widely used as a platform to evaluate PARP inhibitor sensitivity, define structure-function relationships, and prioritize small molecules based on phenotypic rescue [25,33,37]. In this context, MoPARP1-dependent growth inhibition provides a clear and tractable readout that can be leveraged to assess inhibitor responsiveness and guide downstream validation in *M. oryzae*. While compounds identified in yeast would require further characterization for specificity, target engagement, and efficacy in the native pathogen, this approach establishes a foundation for developing chemical probes to interrogate fungal PARP function and explore PARP inhibition as a means to modulate fungal stress responses relevant to pathogenic fitness.

4. Materials and Methods

4.1. Cloning and Vectors

The coding sequences of *M. oryzae* PARP1 (MoPARP1, MGG_08613) and the catalytically inactive mutant MoPARP1-E714A were synthetically generated by Twist Bioscience (San Francisco, CA, USA) and used to generate the expression constructs described in this study. The MoPARP1 and MoPARP1-E714A coding sequences were inserted into the GAL1-driven pESC-LEU vector using a Gibson assembly (GA) approach with NEBuilder HiFi DNA Assembly Master Mix (New England Biolabs, Ipswich, MA, USA), with insertion at the HindIII and XhoI sites (Table S1). The human PARP1 (HsPARP1) coding sequence was obtained from an Addgene plasmid (plasmid #111574) and amplified using Q5 High-Fidelity DNA Polymerase (New England Biolabs, Ipswich, MA, USA) with primers designed to introduce overlaps compatible with GA. The HsPARP1 coding sequence was inserted into the pESC-LEU backbone using GA at the HindIII and XhoI sites. For subcellular localization studies, the MoPARP1 coding sequence was cloned in frame with GFP into the URA3-selectable pD-eGFP vector using GA, with insertion at BamHI and KpnI sites [38]. All constructs were confirmed by whole-plasmid sequencing, performed by Plasmidsaurus (Eugene, OR, USA) using Oxford Nanopore Technology, with custom analysis and annotation, to verify correct insertion, orientation, and in-frame fusion.

4.2. Bacterial Transformation and Plasmid Preparation

Recombinant pESC-LEU and pD-eGFP plasmids were propagated in *Escherichia coli* Top10. Chemically competent Top10 cells were transformed by heat shock at 42 °C for 60 s, recovered in SOC medium at 37 °C for 1 h, and then plated on LB agar containing the appropriate antibiotic. Single colonies were grown overnight at 37 °C in 3–5 mL LB medium with antibiotics, and plasmid DNA was purified using spin miniprep kits. Plasmids were screened by diagnostic restriction digestion and then sequenced to confirm the identity and integrity of MoPARP1, MoPARP1-E714A, and HsPARP1 inserts before yeast transformation.

4.3. Yeast Strains, Media, and Transformation

All yeast experiments were performed in the *S. cerevisiae* strain BY4741 (MATa *his3Δ1 leu2Δ0 met15Δ0 ura3Δ0*) and in an isogenic BY4741-*pdr5*Δ mutant (*YOR153W*; Horizon Discovery, Cambridge, UK), which was used to enhance intracellular accumulation of small-molecule inhibitors in uptake-sensitive assays. For selection of pESC-LEU constructs, strains were maintained on synthetic dropout medium lacking leucine (SD-Leu), whereas

selection of pD-eGFP constructs for localization was carried out on synthetic complete medium lacking uracil (SD-Ura). For repression of GAL1-driven PARP expression, cells were cultured in SD medium supplemented with 2% (*w*/*v*) glucose as the carbon source. For induction of PARP expression, glucose was replaced with 2% (*w*/*v*) galactose. Cultures were routinely grown at 30 °C with shaking at 200 rpm. Yeast transformations were performed using the lithium acetate/polyethylene glycol method. Briefly, BY4741 or BY4741-*pdr5*Δ cultures were grown to mid-log phase (OD_{600} approximately 0.4–0.6), harvested by centrifugation, washed with sterile water, and resuspended in 100 mM lithium acetate. Aliquots of competent cells were mixed with plasmid DNA (typically 200–500 ng), boiled salmon sperm carrier DNA, lithium acetate, and PEG 3350, incubated at 30 °C for 30 min, and subjected to a heat shock at 42 °C for 15 min. Transformed cells were recovered briefly in nonselective medium when needed and plated on SD-Leu or SD-Ura agar for selection. Colonies were re-streaked and verified by colony PCR where necessary. For all experiments, BY4741 WT and BY4741-*pdr5*Δ were transformed with the EV and with each PARP construct.

4.4. Spotting Assays on Glucose and Galactose

The effect of MoPARP1, MoPARP1-E714A, and HsPARP1 expression on yeast growth was assessed by spotting assays under repressing (glucose) and inducing (galactose) conditions. Single colonies from SD-Leu plates were inoculated into 3–5 mL SD-Leu containing 2% glucose and cultured overnight at 30 °C with shaking. Overnight cultures were harvested by centrifugation, washed twice with sterile water to remove residual glucose, and resuspended in sterile water. Cell density was adjusted to OD_{600} = 0.5, and a series of tenfold serial dilutions was prepared. Aliquots of 3 µL from each dilution were spotted onto SD-Leu plates containing either 2% glucose or 2% galactose. Plates were incubated at 30 °C for 48–72 h until colonies were clearly visible, and then photographed. Growth patterns were compared between glucose and galactose for each strain to determine whether induction of PARP expression resulted in growth inhibition. Spotting assays were performed in both BY4741 and BY4741-*pdr5*Δ backgrounds using the same constructs and EV controls.

4.5. Cell Lysis

For yeast cell lysis, 5 mL of galactose-induced cultures was collected, and cells were harvested by centrifugation. Pellets were resuspended in 1 mL 2 M lithium acetate and incubated on ice for 5 min. Samples were pelleted by centrifugation again, and pellets were washed with 0.2 M NaOH with another 5 min incubation on ice. Samples were pelleted, and pellets were resuspended in 60 µL 2X SDS sample buffer (125 mM Tris, pH 6.8, 4% (*w*/*v*) SDS, 20% (*v*/*v*) glycerol, 1 mg/mL bromophenol blue). Protein samples were then heated at 95 °C for 10 min.

4.6. Ribosylation Enrichment

Yeast cells were induced in galactose overnight at a starting OD of 0.3. The next day, the cells were treated with 0.05% MMS for 3 h. Following treatment, yeast cells were pelleted by centrifugation at 3000× *g* for 10 min. Pellets were resuspended in 300 µL protein lysis buffer (50 mM Tris, pH 8, 200 mM NaCl, 1 mM EDTA, 1% (*v*/*v*) Triton-X100, 10% (*v*/*v*) glycerol, 1 mM DTT, 0.5% (*w*/*v*) deoxycholate, Pierce Protease Inhibitor tablet) (Thermo Fisher, Waltham, MA, USA; cat#A32955). Glass beads were added to the lysate and yeast was vortexed at max speed for 10 s with 20 s on ice, repeated 10 times. Lysate was then centrifuged at 2000× *g* for 8 min at 4 °C before being transferred to a new tube and centrifuged at 8000× *g* for 10 min at 4 °C. Lysate was transferred to a new tube, and proteins were quantified using Pierce BCA Protein Assay Kit (Thermo Fisher, Waltham, MA, USA; cat# 23225). In total, 400 µg of yeast lysis was used for enrichment.

For enrichment, agarose Af1521 macrodomain affinity resin (Tulip Biolabs, West Chester, PA, USA; cat# 2302) was used. 20 µL of bead slurry was washed with 1 mL of protein lysis buffer. Beads were spun at max speed for 20 s before supernatant was removed. Beads were then transferred to yeast lysate samples and nutated overnight at 4 °C. The next day, beads were spun at max speed for 20 s, unbound proteins were discarded, and beads were washed 3 times with 1 mL of protein lysis buffer. After the last wash, 75 µL of 1X SDS sample buffer was added to the beads, and the samples were boiled for 10 min at 95 °C.

4.7. Immunoblotting

Proteins were separated by 10% SDS-PAGE and transferred to polyvinylidene difluoride (PVDF) membranes. MoPARP1 expression was detected by immunoblotting using anti-MYC antibody in 3% BSA overnight (1:15,000; clone 9E10, SC-40; Santa Cruz Biotechnology, Dallas, TX, USA). Membranes were washed 3 times for 10 min each using 1X TBST (Thermo Fisher, Waltham, MA, USA; cat#J77500.K2). After washing, membranes were incubated with ProSignal Pico (Genesee, El Cajon, CA, USA; cat#20-300) for 1 min before imaging on an iBright FL 1500 imager (Thermo Fisher, Waltham, MA, USA) for 1–5 min.

For ribosylation enrichment, 20 µL of sample were loaded per well, and proteins were resolved on 10% SDS-PAGE gels. After transfer, membranes were washed 3 times for 1 min with sterile water. Membranes were then stained with Ponceau S (Thermo Fisher, Waltham, MA, USA; cat#A40000279) for 5 min, destained with sterile water, and imaged prior to being destained with 0.1% NaOH for 1 min and rinsed with water. Membranes were incubated with primary anti-poly/mono-ADP ribose antibodies (1:5000; Cell Signaling, Danvers, MA, USA; 89190) in 5% milk overnight. For ribosylation samples, a secondary mouse anti-rabbit IgG-HRP antibody (1:5000; SC2357; Santa Cruz Biotechnology, Dallas, TX, USA) in 5% milk was used for 1 h.

4.8. Liquid Growth Curve Analysis

To quantify the effect of PARP expression on yeast growth, liquid growth curves were generated in microplate format. Overnight cultures grown in SD-Leu containing glucose were harvested, washed twice with sterile water, and diluted into SD-Leu containing 2% galactose to an initial OD_{600} of 0.1. For microplate assays, 100 µL of each culture was dispensed into wells of a sterile 96-well plate in triplicate for each strain and condition. Plates were sealed with a breathable membrane and incubated at 30 °C in a microplate reader with double-orbital shaking at 807 circular movements/min with an orbital diameter of 1 mm (~800 rpm). Optical density at 600 nm was measured every 15 min for 36 h. Growth curves were generated by plotting OD_{600} versus time. Quantitative analysis of growth curves and area under the curve (AUC) measurements was performed using GraphPad Prism version 10.6 (GraphPad Software, Boston, MA, USA).

4.9. Inhibitor Treatment

Pharmacological inhibition of PARP activity in vivo was examined using 3-aminobenzamide (3-AB) and olaparib. A concentrated stock solution of 3-AB was prepared fresh in sterile water, typically at 25 mM. Olaparib was prepared as a concentrated stock solution in DMSO and added to cultures at a final concentration of 25 µM. The concentrations of 3-AB and olaparib were selected based on prior studies demonstrating effective PARP inhibition in yeast and other model systems without nonspecific growth inhibition [21,39,40]. For inhibitor assays, BY4741-*pdr5*Δ strains carrying pESC-LEU EV, MoPARP1-WT, MoPARP1-E714A, or HsPARP1 were grown overnight in SD-Leu with glucose, washed, and resuspended in SD-Leu with galactose to induce PARP expression.

For 3-AB treatment, liquid cultures were supplemented with 3-AB to a final concentration of 5 mM, with equivalent volumes of solvent added to control cultures. For plate-based assays, serial dilution spotting was performed on SD-Leu agar plates containing 5 mM 3-AB. For liquid growth assays, cultures were grown in SD-Leu + galactose in the presence or absence of the inhibitor, as described above, and the OD_{600} was monitored over time. For olaparib treatment, assays were performed exclusively in liquid culture under inducing conditions. Growth was monitored by OD_{600} over time to generate growth curves, and the AUC for each replicate was calculated in GraphPad Prism version 10.6 (GraphPad Software, Boston, MA, USA) and used for quantitative comparison between inhibitor-treated and untreated cultures within each construct. The extent to which olaparib alleviated PARP-dependent growth inhibition relative to untreated controls was used as a measure of inhibitor sensitivity in the yeast system.

4.10. Fluorescence Microscopy for MoPARP1-GFP Localization

Subcellular localization of MoPARP1 was examined in BY4741 cells expressing MoPARP1-GFP from the URA3-selectable pD-eGFP vector. Transformants were grown overnight in SD-Ura medium containing 2% glucose, then shifted to SD-Ura medium containing 2% galactose to induce expression for 6 h at 30 °C. Cells were collected by gentle centrifugation, washed once with 1× phosphate-buffered saline (PBS), and fixed with 4% paraformaldehyde. Following fixation, cells were washed twice with 1× PBS and resuspended in a small volume of PBS. For nuclear staining, Hoechst 33342 (Sigma-Aldrich, St. Louis, MO, USA) was added to the cell suspension to a final concentration of approximately 1 μg/mL and incubated briefly before mounting on microscope slides. Cells were imaged using a fluorescence microscope (Zeiss Axio Observer 7), and representative images were captured. Images were processed using Fiji (ImageJ version 1.54). Raw files were converted to TIFF format, fluorescence channels were split or merged as indicated, and scale bars were added based on image metadata. Only linear brightness and contrast adjustments were applied uniformly across the entire image; no features were added, removed, or otherwise altered.

4.11. Statistical Analysis

All experiments were performed with at least three independent biological replicates. For growth assays, each biological replicate consisted of three technical replicates, which were averaged prior to statistical analysis. Statistical analyses were performed using GraphPad Prism version 10.6 (GraphPad Software, Boston, MA, USA). Differences in growth between strains and conditions were evaluated using two-way ANOVA with strain and treatment as factors. When multiple groups were compared to a single control, Dunnett's multiple-comparisons test was applied; when pairwise comparisons among groups were performed, Šídák's multiple-comparisons test was used. Area under the curve values were calculated from OD_{600} growth curves using the trapezoidal method and are reported as mean ± SD. p values < 0.05 were considered statistically significant.

Supplementary Materials: The following supporting information can be downloaded at: https://www.mdpi.com/article/10.3390/ijms27041901/s1.

Author Contributions: Conceptualization, J.F.; methodology, J.F., N.P. and R.E.K.; writing, J.F., N.P. and R.E.K.; supervision, J.F. All authors have read and agreed to the published version of the manuscript.

Funding: This work received no specific grant from any funding agency. R.E.K. was supported by the University of Florida Office of Research through the Research Opportunity Seed Fund (ROSF).

Institutional Review Board Statement: Not applicable.

Informed Consent Statement: Not applicable.

Data Availability Statement: The original contributions presented in this study are included in the article. Further inquiries can be directed to the corresponding authors.

Acknowledgments: We thank colleagues whose work could not be cited due to space and scope limitations. We thank Adiana Reyes-Kildare and Ethan Scheeler for their technical support. We also thank the Fernandez laboratory for constructive feedback. All figures were created using https://BioRender.com.

Conflicts of Interest: The authors declare no conflicts of interest.

References

1. Aravind, L.; Zhang, D.; de Souza, R.F.; Anand, S.; Iyer, L.M. The natural history of ADP-ribosyltransferases and the ADP-ribosylation system. *Curr. Top. Microbiol. Immunol.* **2015**, *384*, 3–32. [CrossRef]
2. Citarelli, M.; Teotia, S.; Lamb, R.S. Evolutionary history of the poly(ADP-ribose) polymerase gene family in eukaryotes. *BMC Evol. Biol.* **2010**, *10*, 308. [CrossRef]
3. Vyas, S.; Matic, I.; Uchima, L.; Rood, J.; Zaja, R.; Hay, R.T.; Ahel, I.; Chang, P. Family-wide analysis of poly(ADP-ribose) polymerase activity. *Nat. Commun.* **2014**, *5*, 4426. [CrossRef]
4. Lei, P.; Li, W.; Luo, J.; Xu, N.; Wang, Y.; Xie, D.; Guan, H.; Huang, B.; Huang, X.; Zhou, P. PARP (Poly ADP-ribose polymerase) family in health and disease. *MedComm* **2025**, *6*, e70314. [CrossRef]
5. Gupte, R.; Liu, Z.; Kraus, W.L. PARPs and ADP-ribosylation: Recent advances linking molecular functions to biological outcomes. *Genes Dev.* **2017**, *31*, 101–126. [CrossRef] [PubMed]
6. D'Amours, D.; Desnoyers, S.; D'Silva, I.; Poirier, G.G. Poly(ADP-ribosyl)ation reactions in the regulation of nuclear functions. *Biochem. J.* **1999**, *342*, 249–268. [CrossRef] [PubMed Central]
7. Dias, M.P.; Moser, S.C.; Ganesan, S.; Jonkers, J. Understanding and overcoming resistance to PARP inhibitors in cancer therapy. *Nat. Rev. Clin. Oncol.* **2021**, *18*, 773–791. [CrossRef] [PubMed]
8. Hu, M.L.; Pan, Y.R.; Yong, Y.Y.; Liu, Y.; Yu, L.; Qin, D.L.; Qiao, G.; Law, B.Y.; Wu, J.M.; Zhou, X.G.; et al. Poly (ADP-ribose) polymerase 1 and neurodegenerative diseases: Past, present, and future. *Ageing Res. Rev.* **2023**, *91*, 102078. [CrossRef] [PubMed]
9. O'Malley, D.M.; Krivak, T.C.; Kabil, N.; Munley, J.; Moore, K.N. PARP inhibitors in ovarian cancer: A review. *Target. Oncol.* **2023**, *18*, 471–503. [CrossRef]
10. Lee, J.M.; Ledermann, J.A.; Kohn, E.C. PARP Inhibitors for BRCA1/2 mutation-associated and BRCA-like malignancies. *Ann. Oncol.* **2014**, *25*, 32–40. [CrossRef]
11. Farmer, H.; McCabe, N.; Lord, C.J.; Tutt, A.N.; Johnson, D.A.; Richardson, T.B.; Santarosa, M.; Dillon, K.J.; Hickson, I.; Knights, C.; et al. Targeting the DNA repair defect in BRCA mutant cells as a therapeutic strategy. *Nature* **2005**, *434*, 917–921. [CrossRef]
12. Block, M.D.; Verduyn, C.; Brouwer, D.D.; Cornelissen, M. Poly(ADP-ribose) polymerase in plants affects energy homeostasis, cell death and stress tolerance. *Plant J.* **2005**, *41*, 95–106. [CrossRef]
13. Feng, B.; Liu, C.; de Oliveira, M.V.V.; Intorne, A.C.; Li, B.; Babilonia, K.; de Souza Filho, G.A.; Shan, L.; He, P. Protein Poly(ADP-ribosyl)ation regulates *Arabidopsis* immune gene expression and defense responses. *PLoS Genet.* **2015**, *11*, e1004936. Erratum in *PLoS Genet.* **2016**, *12*, e1005294. [CrossRef] [PubMed]
14. Song, J.; Keppler, B.D.; Wise, R.R.; Bent, A.F. PARP2 is the predominant Poly(ADP-Ribose) polymerase in *Arabidopsis* DNA damage and immune responses. *PLoS Genet.* **2015**, *11*, e1005200. [CrossRef]
15. Nalley, L.; Tsiboe, F.; Durand-Morat, A.; Shew, A.; Thoma, G. Economic and environmental impact of rice blast pathogen (*Magnaporthe oryzae*) alleviation in the United States. *PLoS ONE* **2016**, *11*, e0167295. [CrossRef]
16. Pennisi, E. Armed and dangerous. *Science* **2010**, *327*, 804–805. [CrossRef] [PubMed]
17. Yan, X.; Tang, B.; Ryder, L.S.; MacLean, D.; Were, V.M.; Eseola, A.B.; Cruz-Mireles, N.; Foster, A.J.; Osés-Ruiz, M.; Talbot, N.J. The transcriptional landscape of plant infection by the rice blast fungus *Magnaporthe oryzae* reveals distinct families of temporally co-regulated and structurally conserved effectors. *Plant Cell* **2023**, *35*, 1360–1385. [CrossRef]
18. Fernandez, J.; Orth, K. Rise of a cereal killer: The biology of *Magnaporthe oryzae* biotrophic growth. *Trends Microbiol.* **2018**, *26*, 582–597. [CrossRef]
19. Cruz-Mireles, N.; Eseola, A.B.; Osés-Ruiz, M.; Ryder, L.S.; Talbot, N.J. From appressorium to transpressorium—Defining the morphogenetic basis of host cell invasion by the rice blast fungus. *PLoS Pathog.* **2021**, *17*, e1009779. [CrossRef] [PubMed]
20. Ryder, L.S.; Cruz-Mireles, N.; Molinari, C.; Eisermann, I.; Eseola, A.B.; Talbot, N.J. The appressorium at a glance. *J. Cell Sci.* **2022**, *135*, jcs259857. [CrossRef]
21. Gao, X.; Gao, G.; Zheng, W.; Liu, H.; Pan, W.; Xia, X.; Zhang, D.; Lin, W.; Wang, Z.; Feng, B. PARylation of 14-3-3 proteins controls the virulence of *Magnaporthe oryzae*. *Nat. Commun.* **2024**, *15*, 8047. [CrossRef]

22. Wang, J.; Gao, Y.; Xiong, X.; Yan, Y.; Lou, J.; Guo, M.; Noman, M.; Li, D.; Song, F. Poly(ADP-ribose) polymerase FonPARP1-catalyzed PARylation of protein disulfide isomerase FonPdi1 regulates pathogenicity of *Fusarium oxysporum* f. sp. niveum on watermelon. *Int. J. Biol. Macromol.* **2025**, *291*, 139046. [CrossRef]
23. Wang, J.; Gao, Y.; Xiong, X.; Yan, Y.; Lou, J.; Noman, M.; Li, D.; Song, F. The Ser/Thr protein kinase FonKin4-poly(ADP-ribose) polymerase FonPARP1 phosphorylation cascade is required for the pathogenicity of watermelon fusarium wilt fungus *Fusarium oxysporum* f. sp. niveum. *Front. Microbiol.* **2024**, *15*, 1397688. [CrossRef]
24. Vanderwaeren, L.; Dok, R.; Voordeckers, K.; Nuyts, S.; Verstrepen, K.J. *Saccharomyces cerevisiae* as a model system for eukaryotic cell biology, from cell cycle control to DNA damage response. *Int. J. Mol. Sci.* **2022**, *23*, 11665. [CrossRef]
25. Rissel, D.; Heym, P.P.; Peiter, E. A yeast growth assay to characterize plant poly(ADP-ribose) polymerase (PARP) proteins and inhibitors. *Anal. Biochem.* **2017**, *527*, 20–23. [CrossRef]
26. Kaiser, P.; Auer, B.; Schweiger, M. Inhibition of cell proliferation in *Saccharomyces cerevisiae* by expression of human NAD+ ADP-ribosyltransferase requires the DNA binding domain ("zinc fingers"). *Mol. Gen. Genet. MGG* **1992**, *232*, 231–239. [CrossRef] [PubMed]
27. Tao, Z.; Gao, P.; Liu, H.-w. Studies of the expression of human poly(ADP-ribose) polymerase-1 in *Saccharomyces cerevisiae* and Identification of PARP-1 substrates by yeast proteome microarray screening. *Biochemistry* **2009**, *48*, 11745–11754. [CrossRef]
28. Langelier, M.F.; Planck, J.L.; Roy, S.; Pascal, J.M. Structural basis for DNA damage-dependent poly(ADP-ribosyl)ation by human PARP-1. *Science* **2012**, *336*, 728–732. [CrossRef] [PubMed]
29. Obaji, E.; Haikarainen, T.; Lehtiö, L. Characterization of the DNA dependent activation of human ARTD2/PARP2. *Sci. Rep.* **2016**, *6*, 34487. [CrossRef]
30. Perkins, E.; Sun, D.; Nguyen, A.; Tulac, S.; Francesco, M.; Tavana, H.; Nguyen, H.; Tugendreich, S.; Barthmaier, P.; Couto, J.; et al. Novel inhibitors of poly(ADP-ribose) polymerase/PARP1 and PARP2 identified using a cell-based screen in yeast. *Cancer Res.* **2001**, *61*, 4175–4183. [PubMed]
31. Sepšiová, R.; Procházková, K.; Červenák, F.; Majerčík, D.; Hanáková, K.; Lattová, E.; Hajikazemi, M.; Zdráhal, Z.; Virágová, S.; Brzáčová, Z.; et al. Poly (ADP-ribose) polymerase in yeasts: Characterization and involvement in telomere maintenance. *Nucleic Acids Res.* **2025**, *53*, gkaf837. [CrossRef] [PubMed]
32. Popova, L.G.; Khramov, D.E.; Nedelyaeva, O.I.; Volkov, V.S. Yeast heterologous expression systems for the study of plant membrane proteins. *Int. J. Mol. Sci.* **2023**, *24*, 10768. [CrossRef]
33. Brown, G.W.; Andrews, B. Setting molecular traps in yeast for identification of anticancer drug targets. *Proc. Natl. Acad. Sci. USA* **2021**, *118*, e2105547118. [CrossRef] [PubMed]
34. La Ferla, M.; Mercatanti, A.; Rocchi, G.; Lodovichi, S.; Cervelli, T.; Pignata, L.; Caligo, M.A.; Galli, A. Expression of human poly (ADP-ribose) polymerase 1 in *Saccharomyces cerevisiae*: Effect on survival, homologous recombination and identification of genes involved in intracellular localization. *Mutat. Res. —Fundam. Mol. Mech. Mutagen.* **2015**, *774*, 14–24. [CrossRef]
35. Eguchi, Y.; Makanae, K.; Hasunuma, T.; Ishibashi, Y.; Kito, K.; Moriya, H. Estimating the protein burden limit of yeast cells by measuring the expression limits of glycolytic proteins. *eLife* **2018**, *7*, e34595. [CrossRef]
36. Kastberg, L.L.B.; Ard, R.; Jensen, M.K.; Workman, C.T. Burden imposed by heterologous protein production in two major industrial yeast cell factories: Identifying sources and mitigation strategies. *Front. Fungal Biol.* **2022**, *3*, 827704. [CrossRef]
37. Menacho-Márquez, M.; Murguía, J.R. Yeast on drugs: *Saccharomyces cerevisiae* as a tool for anticancer drug research. *Clin. Transl. Oncol.* **2007**, *9*, 221–228. [CrossRef]
38. Schindelin, J.; Arganda-Carreras, I.; Frise, E.; Kaynig, V.; Longair, M.; Pietzsch, T.; Preibisch, S.; Rueden, C.; Saalfeld, S.; Schmid, B.; et al. Fiji: An open-source platform for biological-image analysis. *Nat. Methods* **2012**, *9*, 676–682. [CrossRef] [PubMed]
39. Kukolj, E.; Kaufmann, T.; Dick, A.E.; Zeillinger, R.; Gerlich, D.W.; Slade, D. PARP inhibition causes premature loss of cohesion in cancer cells. *Oncotarget* **2017**, *8*, 103931–103951. [CrossRef]
40. Rajawat, J.; Awasthi, P.; Banerjee, M. PARP inhibitor olaparib induced differential protein expression in cervical cancer cells. *J. Proteom.* **2023**, *275*, 104823. [CrossRef]

Disclaimer/Publisher's Note: The statements, opinions and data contained in all publications are solely those of the individual author(s) and contributor(s) and not of MDPI and/or the editor(s). MDPI and/or the editor(s) disclaim responsibility for any injury to people or property resulting from any ideas, methods, instructions or products referred to in the content.